Strain Effect On the Perpendicular Magnetization Switching Driven by Spin-Orbit Torque

Yuzhe Chen, \$^1,2,3\$ Zhuoyi Li, \$^1,2,3\$ Zhe Zhang, \$^1,2,3\$ Sicong Hu, \$^1,2,3\$ Zhihao Li, \$^1,2,3\$ Junwei Hou, \$^4\$ Lei Wang, \$^5\$ Yu Yan, \$^2\$ Yao Li, \$^1,2,3\$ Liang He, \$^1,2,3\$ Jun Du, \$^1,6\$ Rong Zhang, \$^1,6\$ Jing Wu, \$^7,8\$ Xianyang Lu, \$^1,2,3,a\$) Hang Xie, \$^1,3,b\$) and Yongbing Xu 1,2,3,4,c)

¹⁾National Key Laboratory of Spintronics, Nanjing University, Suzhou 215163, China.

³⁾School of Integrated Circuits, Nanjing University, Suzhou 215163, China.

In this study, we investigate the influence of strain on spin-orbit torque and current-induced magnetization switching in Ta/Pt/Co/Ta heterostructures deposited on flexible polyimide substrates. By applying strain ranging from -12.5% (compressive) to 12.5% (tensile), we observe that increasing the strain amplitude reduces coercivity and enhances spin-orbit torque efficiency, collectively leading to a 28.6% reduction in switching current density. The lowest achieved switching current density is 3.07 MA/cm². Our findings demonstrate strain-mediated tuning of spin-orbit torque and underscore the potential of such heterostructures for flexible spintronic applications.

Key words: strain, spin-orbit torque, flexible substrate, coercivity,damping-like torque.

Spin-orbit torque (SOT), originated from spin Hall effect (SHE) in bulk non-magnet metal (NM) or Rashba-Edelstein effect (REE) at the interface, allows effective electrical manipulation of magnetization state in the ferromagnetic layer (FM), with ultrafast speed and lower power consumption^{1–7}. Furthermore, the separated write path from the read path greatly reduces the breakdown risk of tunnel barrier in the magnetic tunnel junction (MTJ), and thus increases the device durability of SOT-based magnetic random access memory^{8–11}.

In addition to the memory device, the last decade has also witnessed the potential of SOT in other applications, such as nano-oscilators 12-14, quantum computing 15,16, magnetic sensors^{17–21}. Nowadays, the wearable and flexible electronic devices are becoming trendy and demanding^{22–25}. The SOTbased devices are also expected to fit in the application scenario that requires flexibility. Therefore, it is important to investigate the SOT efficiency in conventional SOT stacks fabricated on flexible substrates. Attempts have been made to demonstrate the good repeatability of flexible SOT spin logic device through 100 cycles of bending²⁶. In addition, spintransfer ferromagnetic resonance (ST-FMR) was employed to characterize SOT efficiency of devices on flexible substrate, from which enhanced SOT was observed after application of tensile or compressive strain^{27,28}. Notably, strain engineering has been shown to significantly tune critical properties of spin devices, including exchange bias field²⁹, Gilbert damping³⁰, spin-orbit coupling³¹ and magnetic anisotropy^{32,33}. Despite these efforts, the research on flexible SOT-based devices is still lacking, and detailed effect of strain (both tensile and compressive) in SOT amplitude and current-induced switching is still to be understood.

In this work, we study the strain effect in magnetic property and SOT of Ta/Pt/Co/Ta stacks deposited on polyimide substrates. Compressive and tensile strains were applied on the substrates with maximum curvature radius of 20 mm, corresponding to strain of 12.5%. It is found that both compressive and tensile strains lead to decrease of coercivity and anomalous Hall resistance amplitude. On the other hand, dampinglike (DL) and field-like (FL) SOT efficiencies also exhibit changes after the application of strain, though the influence in SOT under compression strain is less prominent. By further performing current-induced switching measurement, we observed continuous reduction of critical current density as the increase of applied strain, which corroborates well with the AHE and SOT characterization results and can be attributed to both the reduction in coercivity and enhancement of SOT. The reduction reaches maximum 28.6% at a tensile strain of 12.5%. Our study shows the great potential of SOT stacks to be implemented in flexible device applications.

All the samples were grown on a 125- μ m-thick flexible polyimide substrate. The atomic force microscopy (AFM) test showed that the roughness of the substrate was 0.79 nm (see Fig. S2). Thin film stacks of Ta(1)/Pt(4)/Co(0.8)/Ta(6) were deposited directly on the polyimide substrate using a magnetron sputtering system at room temperature (the numbers

²⁾ Jiangsu Provincial Key Laboratory of Advanced Photonic and Electronic Materials, School of Electronic Science and Engineering, Nanjing University, Nanjing 210093, China.

⁴⁾York-Nanjing International Center for Spintronics (YNICS), School of Physics, Engineering and Technology, University of York, York YO10 5DD, UK.

⁵⁾Key Laboratory of Quantum Materials and Devices of Ministry of Education, School of Physics, Southeast University, Nanjing 211189, China.

⁶⁾National Laboratory of Solid State Microstructures, Nanjing University, Nanjing 210093, China

⁷⁾School of Integrated Circuits, Guangdong University of Technology, Guangzhou 510006, China.

⁸⁾ York-Nanjing International Center for Spintronics (YNICS), School of Physics, Engineering and Technology, University of York, York YO10 5DD, UK

a) Electronic mail: xylu@nju.edu.cn b) Electronic mail: xiehang@nju.edu.cn

c)Electronic mail: ybxu@nju.edu.cn

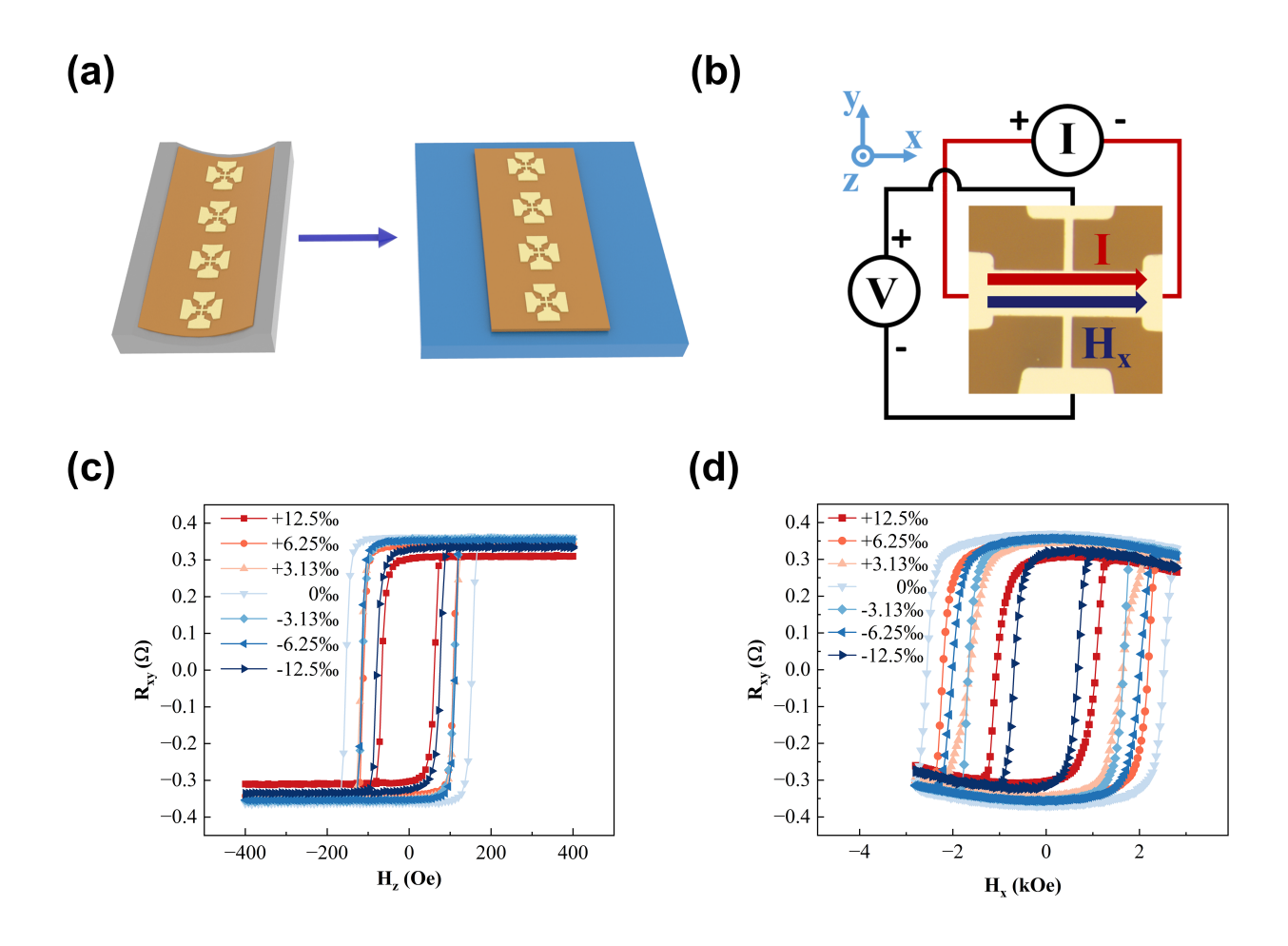


FIG. 1. (a) Schematic of the strain engineering process. The flexible substrate is fixed on a mold during film deposition and flattened to induce strain in the magnetic film. (b) Schematic of configuration for electric measurement. Hall resistance as a function of (c) out-of-plane field H_z and (d) in-plane field H_x under varied strain from -12.5% to 12.5%.

in parentheses denote thickness in nanometers). The working and base pressure are 7 mTorr and $<1\times10^{-8}$ Torr. As illustrated in Fig. 1a, during the film deposition, the flexible substrates were firstly bent and fixed onto self-made convex or concave aluminum molds with diverse curvature radii. This operation induces either compressive or tensile strains in the thin films, which were then flattened by a self-assembled tool kit and further attached to a solid substrate (see Supplementary Information S1 for more detailed design). The above procedure is crucial as it enables the generation of the desired strain conditions for the magnetic film's subsequent performance and property analysis. To facilitate the electrical measurement, the films were subsequently patterned into Hall bars using ultraviolet lithography followed by ion etching. The size of the central squares of these Hall bars is 30 μ m×5 μ m. A Keithley 6221 source meter and a Keithley 2182 nanovoltmeter were employed to apply the current and measure the voltage during electrical measurement.

We firstly examined the thin film resistivity along the direction of applied strain. It was found that the resistance value exhibited a nearly linear relationship with the strain from -12.5% to +12.5% (see Supplementary Information S3). This phenomenon can be attributed to the macroscopic deformation of the resistor length, which corresponds to the lattice strain in a microscopic picture. We further performed the anomalous Hall effect (AHE) measurements at different applied strains to study the magnetic property of the SOT stack on flexible substrate (see Fig. 1b for measurement configuration). Figure 1c shows the AHE resistances of the device as a function the outof-plane magnetic field at different strains. As can be seen, the AHE loop of the device has clear hysteresis throughout the strain range, indicating the SOT stack maintains good perpendicular magnetic anisotropy(PMA) on polyimide substrate. In addition, it also implies that the polyimide substrate allows continuous ultrathin film deposition required for formation of strong PMA.

Despite the clear hysteresis in PMA, we can find that the strains affect the detailed shape of the AHE loop in the thin film. Specifically, a larger strain leads to a reduction in both the coercivity and the AHE amplitude. The latter can be at-

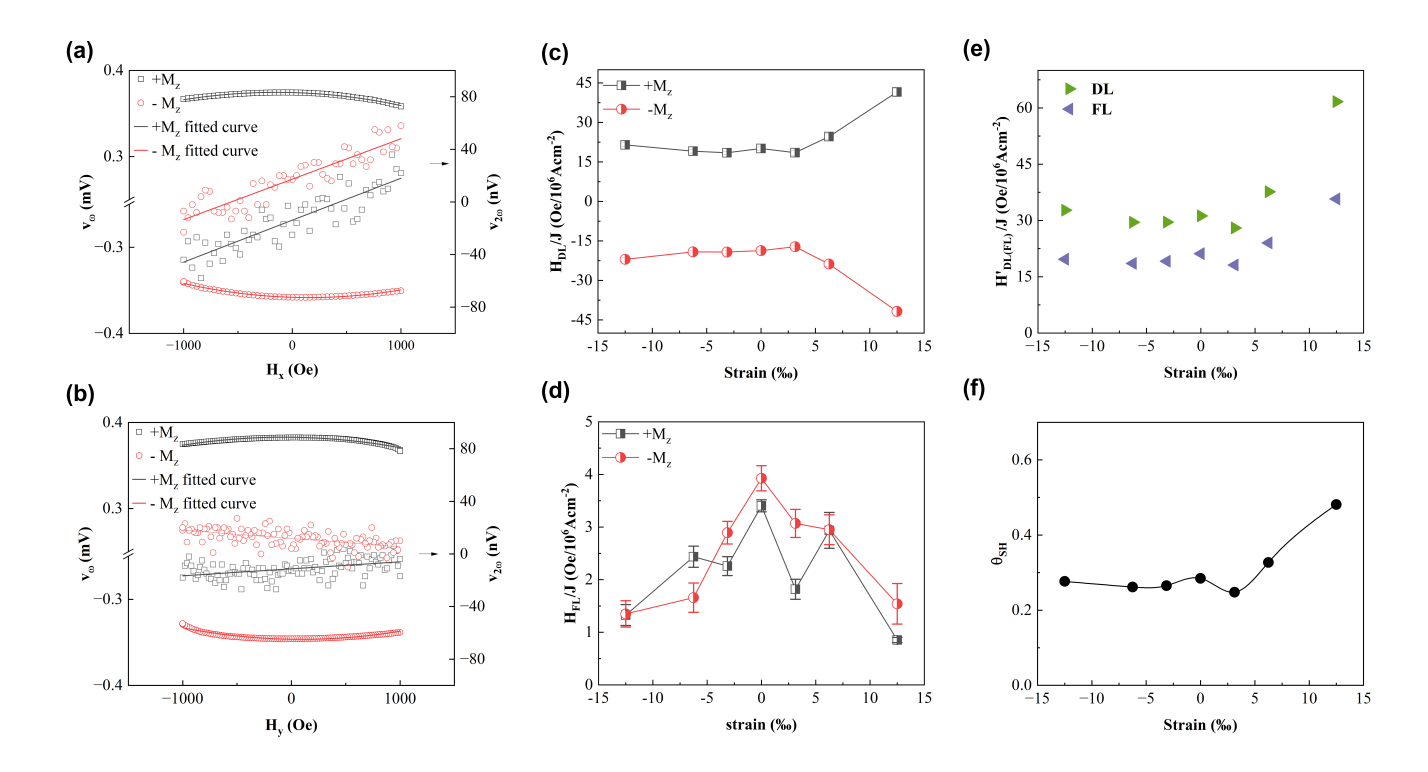


FIG. 2. First and second harmonic Hall voltages as a function of (a) H_x and (b) H_y for Polyimide/Ta/Pt/Co/Ta at zero strain. The current amplitude is 1 mA, corresponding to current density of around $2.82 \times 10^5 \,\mathrm{A/cm^2}$. (c)-(d) Extracted DL and FL SOT Effective fields H_{DL} and H_{FL} of the sample at different strains, respectively. (e) SOT effective fields $H'_{DL(FL)}$ after the PHE correction. (f) Calculated spin Hall angle as a function of strain.

tributed to both the thin film resistivity reduction and magnetization decrease, while the former may not be directly related to the PMA strength. To further investigate the strain effect on the perpendicular anisotropy, we also performed AHE measurement under the in-plane magnetic field along x-axis. The field is slightly titled towards the out-of-plane direction with tilt angle of 3 - 5° to assist complete switching of the magnetic domains. The coercivity here can be easily affected by the slight variation of tilt angle and domain wall nucleation-propagation process. Therefore, it may not follow the same Hc-strain relationship as the one shown in Fig. 1c. From the curvature of AHE loop obtained under inplane magnetic field as shown in Fig. 1d, we could estimate the effective anisotropy field $H_{k,eff}$ via fitting. The detailed fitting procedure can be found in the Supplementary Informaition S4. Overall, strain leads to a noticeable reduction in coercivity and magnetization, the strength of PMA remains a similar level, which shows no clear dependence on the strain. These findings are further corroborated by vibrating sample magnetometer (VSM) measurements (see Fig. S5). Co thin film has a relatively large negative magnetoelastic constant of -7×10^{-5} , 34 and therefore the in-plane strain would affect the magnetic property theoretically. Such effect may be less prominent for ultrathin Co films used in our study due to its polycrystalline structure with smaller magnetoelastic constant than that of single crystalline Co. In addition, such effect may be mainly shown on magnetization and coercivity, which however becomes negligible on the anisotropy strength. This may be due to the fact that the PMA in the structure originates from the electronic band hybridization of Pt and Co at the interface, and the strain within the range of $\pm 12.5\%$ does not cause evident degradation of the interface.

Thereafter, We performed harmonic Hall voltage measurements to characterize SOT for the above thin film. Putting aside the detailed origin, there are generally two types of SOT in a magnetic heterostructure - field-like SOT and dampinglike SOT. The direction of former is given by $\overrightarrow{\tau}_{FL} \propto \hat{\sigma} \times \overrightarrow{m}$, while the latter has a direction along $\overrightarrow{\tau}_{DL} \propto \overrightarrow{m} \times (\hat{\sigma} \times \overrightarrow{m})$, where $\hat{\sigma}$ and \overrightarrow{m} represent spin polarization of the spin current and magnetization direction of the FM layer, respectively. From the above relationships, the DL SOT and FL SOT have different symmetry with respect to the magnetization. The corresponding effective field of DL SOT, H_{DL} , depends on the magnetization direction, whereas the effective FL SOT field $H_{\rm FL}$ does not change direction with magnetization. During harmonic Hall voltage measurements, an ac current I_{AC} with fixed frequency of 133 Hz and varied amplitude is applied to the long axis of Hall bar. The first and second harmonic Hall voltages are measured simultaneously by a lock-in amplifier, as a function of the in-plane magnetic field H_x (for DL SOT) or H_v (for FL SOT) sweeping between -1000 Oe and 1000 Oe back and forth. The impedance mismatch/capacitive coupling and thermal effects during measurements are negligible due to the low frequency and small amplitude of current used,

respectively.

Figure 2 a,b show the first and second harmonic Hall voltages $(V_{\omega} \text{ and } V_{2\omega})$ versus in-plane field H_x and H_y for polyimide/Ta/Pt/Co/Ta stacks without applied strain, respectively. As can be seen, the first harmonic voltage shows a parabolic shape with the in-plane field, while the second harmonic voltage is linear with the in-plane field. The values of H_{DL} and H_{FL} can be then extracted by fitting the curves in the small magnetic field range using the following equation:

$$H_{\rm DL(FL)} = -2 \frac{dV_{2\omega}/dH_{x(y)}}{d^2 V_{\omega}/dH_{x(y)}^2}$$
 (1)

The extracted $H_{\rm DL}$ and $H_{\rm FL}$ at different current density is shown in Fig. S6, from which we could further obtain the SOT effective field per current density $H_{\rm DL}/J$ and $H_{\rm FL}/J$. By applying strain to the sample and repeating the above SOT characterization at varied strain, we find that the $H_{\rm DL}/J$ enhances as the increase of tensile strain, though the enhancement of $H_{\rm DL}/J$ under compression strain is less evident compared with the tensile strain case (Fig. 2c). As for $H_{\rm FL}/J$, it decreases at either compression or tensile strain. Considering the possible deviation induced by the planar Hall effect (PHE) during harmonic SOT characterization, we further added PHE correction for SOT value extraction by employing the equation,

$$H'_{\rm DL(FL)} = \frac{H_{\rm DL(FL)} + 2\xi H_{\rm FL(DL)}}{1 - 4\xi^2}$$
 (2)

where the $H'_{\rm DL(FL)}$ is the DL (FL) SOT effective field after the correction, the ratio of AHE and PHE resistance change $\xi = \Delta R_{\rm P}/\Delta R_{\rm A}$ is determined to be 0.28 (see Supplementary Information S7). The relatively large ξ value in our samples can lead to non-negligible underestimation of SOT. The SOT effective fields per current density after PHE-correction are plotted in Fig. 2e, from which we can find that the SOT significantly improves after the tensile strain is applied, while the effect of compressive strain on SOT is nearly negligible.

With the extracted SOT effective field, we further calculated the spin Hall angle θ_{SH} using the expression θ_{SH} = $\frac{2e}{\hbar}M_{\rm S}t\frac{H_{\rm DL}'}{i}$, where e is the electron charge, \hbar is the planck constant, M_s is the saturation magnetization of the sample at different strains. It should be noted that the AHE resistance values $\Delta R_{\rm A}$ also changes after the strain is applied, as shown in Fig. 1c. Considering that the ΔR_A scales with the perpendicular component of the saturation magnetization³⁵, the AHE resistance decrease as the strain increases can be caused by the magnetization reduction due to the magnetostrictive effect. Thereafter, we used the saturation magnetization $M_{s,0}$ obtained from the VSM measurement at zero strain as the reference, and estimated the saturation magnetization M_s of the sample at different strains using the relationship of $M_s = M_{s,0} \Delta R_A / \Delta R_{A,0}$, where $\Delta R_{A,0}$ is the AHE resistance change at zero strain. By taking the estimated M_s into the above equation, we could obtain the spin Hall angle at varied strain. As shown in Fig. 2f, similar as the trend for SOT, the spin Hall angle greatly increases as the increase of tensile strain, while the compressive strain has very limited effect on its level. In addition, the relatively high θ_{SH} value in our study can be ascribed to the presence of Pt and Ta layers with opposite spin hall angle at the two sides of ferromagnetic layer, and therefore the spin currents from the two layers will add up.

The observed enhancement of spin Hall angle under tensile strain may result from the combined action of the bulk effect and the interface effect due to Pt, Ta lattice deformation. Theoretical study has reported that the tensile strain is able to induce a large Rashba spin splitting at the valence band maximum of the 2D GeTe monolayer, leading to a large Rashba coefficient of up to 1.98 eVÅ³⁶. This study further pointed out that the detailed origin of the Rashba effect can be from the enhanced vertical potential gradient due to the out-of-plane orbital component induced by tensile strain. Importantly, an earlier experimental study also found that the interface/surface vertical potential gradient can bring about strong Rashba effect, further increasing the SOT in the HM/FM system³⁷. On the other hand, from the first-principle calculations, the compression strain does not have such effect on band structure, and thus does not lead to enhanced Rashba effect. The above observation is consistent with our results. The strain effect on Rashba spin splitting may also apply to the HM/FM heterostructures, which well account for the observed enhancement of spin Hall angle under tensile strain in our study. Further study is required to calculate the strain effect on Rashba effect in HM/FM interface. In addition, as aforementioned, we do not rule out the possible contribution from bulk effects such as SHE and orbital Hall effect (OHE) due to tensile strain. In future study, one may employ non-local lateral spin valve transport³⁸, X-ray magnetic circular dichroism (XMCD)³⁹, or spatially resolved magneto-optic Kerr effect (MOKE) measurements^{40,41} to directly probe spin or orbital current generation at different strains, and further disentangle the contribution from bulk and interface effects.

Next, we proceeded to the current-induced switching measurement, in which a pulsed current (I_{pulse}) with pulse width of 100 µs and varied amplitude from -20 mA to 20 mA are injected in the longitudinal direction of the Hall bar. Following each pulse, the Hall voltage was measured with a small reading current of 200 μ A. A fixed in-plane auxiliary field (H_x) is applied along the current direction during each measurement to break the symmetry. Figure 3a shows current-induced switching loops of the polyimide/Ta/Pt/Co/Ta at different inplane auxiliary field with zero strain (left panel) and 12.5% strain (right panel). Deterministic switching was observed for both cases - the switching polarity reverses as the direction of either the current or in-plane field reverses. The switching symmetry is consistent with previous observed SOT-induced perpendicular magnetization switching for Pt/Co stacks. The switching amplitude is nearly zero when the in-plane field is absent, which gradually increases as the field increases and eventually reaches a saturated level. Additionally, we also observed evident current-induced switching for the sample under the MOKE microscope, with the switching polarity consistent with electrical measurement. The smaller contrast in the MOKE images exhibited in sample under high tensile strain

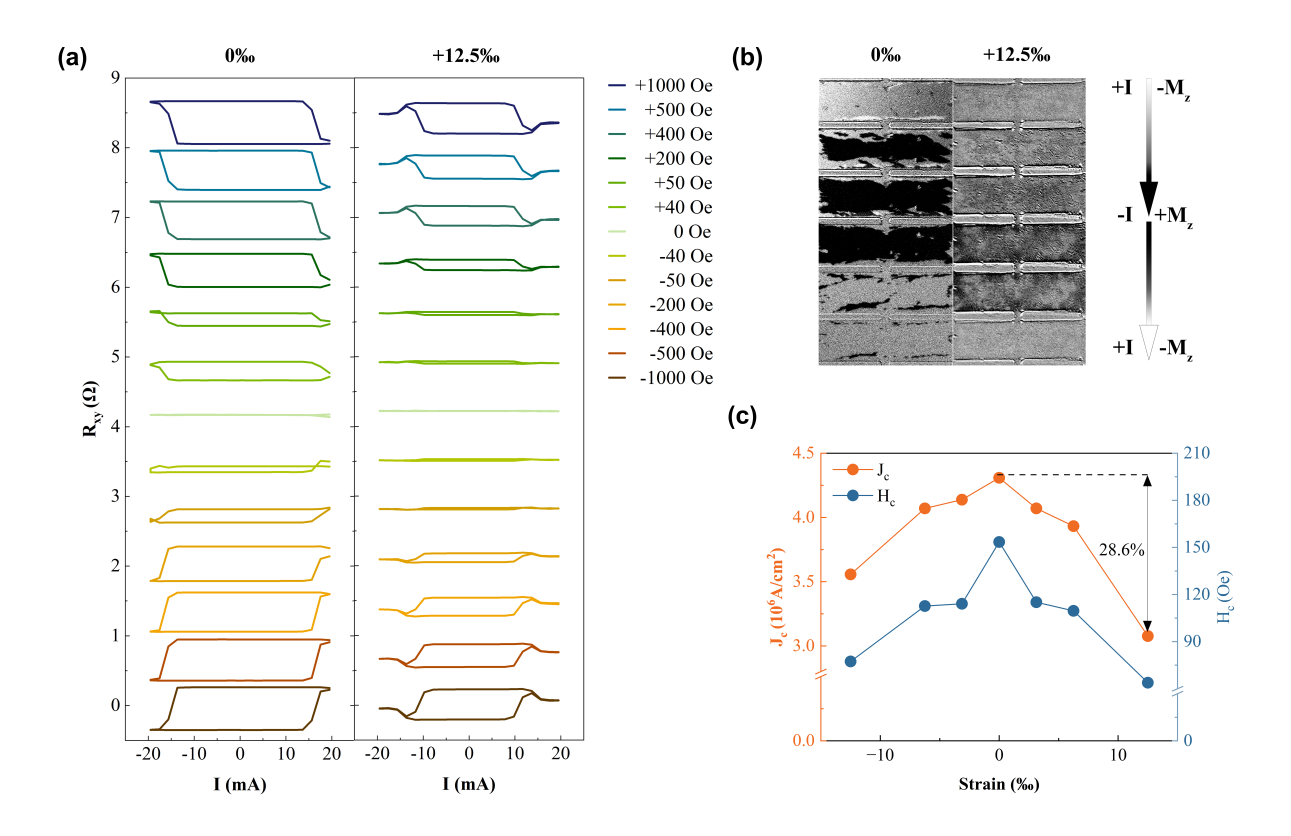


FIG. 3. (a) Current-induced switching loops of Polyimide/Ta/Pt/Co/Ta structure at strain level of 0 and +12.5%, with various in-plane auxiliary field from -1000 Oe to 1000 Oe. (b) MOKE images of the sample with strains of 0 and +12.5% at in-plane auxiliary field of 1000 Oe.(c) Extracted critical current density and coercivity from current-induced and field-induced switching loops for the sample at varied strains.

might be related to the reduced switching ratio. Under large strain and in-plane magnetic field, magnetic domains tend to remain in a multi - domain state.

We further extracted the switching current density J_c at each strain under an in-plane magnetic field of 1000 Oe and plotted in Fig. 3c. For specific switching curves at varied strains, one can refer to Fig. S11. Since the strain affects the coercivity of the sample, which may in turn affect the critical current density in current-induced switching, we also plotted the coercivity as a function of strain together. Clearly, both the compressive and tensile strain can lead to evident reduction in the critical current density. Additionally, we can also observe a good correlation between J_c and coercivity. In the case of tensile strain, J_c drops by 28.6% from 4.30 $\times 10^6$ A/cm² to $3.07 \times 10^6 \text{A/cm}^2$ as the strain increases to +12.5%, accompanied by 58.4% reduction in coercivity of AHE loop. On the other hand, under compressive strain, the coercivity decreases by 49.6% and J_c decreases by 17.5%. The larger reduction of critical current density under tensile strain than the compressive strain case can be attributed to the enhanced spin Hall angle as discussed above. It should also be noted that the thermal effect should also play a role in assisting the switching (see Supplementary Information S9 for details), which should not vary significantly at different strains and therefore will not affect the analysis of strain effect on SOT and switching.

In summary, we studied the strain effect on spin-charge

conversion efficiency in Ta/Pt/Co/Ta thin film deposited on flexible polyimide substrate. It is found that the tensile strain leads to enhanced spin Hall angle by 69% within the applied strain range, while compression strain has negligible effect on the SOT efficiency of the thin film. We further demonstrated electrical manipulation of perpendicular magnetization state of the stack, and observed reduced critical current density at both compression and tensile strain, which can be largely attributed to the reduced coercivity. Under tensile strain, due to enhanced spin Hall angle, such reduction is even more evident with a 28.6% reduction of switching current density at strain level of +12.5%. Our work not only unveils the positive effect of tensile strain in promoting SOT generation, but also highlights the potential of the SOT-based spintronic devices to be employed in flexible and wearable application scenarios.

ACKNOWLEDGMENTS

This work was supported by the National Key Research and Development Program of China (Grant No. 2021YFB3601600), the National Natural Science Foundation of China (Grant Nos. 12104216, 12241403, and 61427812), and the Natural Science Foundation of Jiangsu Province of China (Nos. BK20200307, BK20192006, and BK20180056).

AUTHOR DECLARATIONS

Conflict of Interest

The authors have no conflicts to disclose.

Author Contributions

Yuzhe Chen: Conceptualization (lead); Data curation (lead); Formal analysis (lead); Investigation (lead); Methodology (lead); Project administration (lead); Software (equal); Supervision (lead); Validation (lead); Visualization (lead); Writing - original draft (lead); Writing review & editing Zhuoyi Li: Methodology (supporting); Software (supporting); Writing – review & editing (supporting). **Zhe Zhang:** Conceptualization (supporting); Data curation (supporting); Formal analysis (supporting); Investigation (supporting). Sicong Hu:Formal analysis (supporting); Investigation (supporting). **Zhihao Li:** Data curation (supporting): Resources (supporting). Junwei Hou: Data curation (supporting). Lei Wang: Software (equal). Yan Yu: Formal analysis (supporting). Yao Li: Supervision (supporting). Liang He: Resources (supporting); Supervision (supporting). Jun Du: Formal analysis (supporting). Rong Zhang: Resources (supporting). Jing Wu: Formal analysis (supporting).

Xianyang Lu: Conceptualization (equal); Data curation (equal); Formal analysis (equal); Funding acquisition (equal); Investigation (equal); Methodology (equal); Project administration (equal); Resources (lead); Validation (equal); Writing – review & editing (equal). Hang Xie: Investigation (equal); Methodology (equal); Project administration (equal); Validation (equal); Writing – review & editing (equal). Yongbing Xu: Conceptualization (supporting); Data curation (supporting); Formal analysis (supporting); Funding acquisition (lead); Investigation (equal); Project administration (lead); Resources (lead); Writing – review & editing (equal).

DATA AVAILABILITY

The data that support the findings of this work are available within the paper and its Supplementary Information. Additional data are available from the corresponding authors upon reasonable request.

REFERENCES

- ¹L. Zhu, Advanced Materials **35**, 2300853 (2023).
- ²S. Bhatti, R. Sbiaa, A. Hirohata, H. Ohno, S. Fukami, and S. N. Piramanayagam, Materials Today 20, 530 (2017).
- ³J. Ryu, S. Lee, K.-J. Lee, and B.-G. Park, Advanced Materials **32**, 1907148 (2020).
- ⁴J. Zhou and J. Chen, Advanced Electronic Materials 7, 2100465 (2021).
- ⁵S. Ikegawa, F. B. Mancoff, J. Janesky, and S. Aggarwal, IEEE Transactions on Electron Devices 67, 1407 (2020).
- ⁶M. Yang, Y. Cui, J. Chen, and J. Luo, International Journal of Extreme Manufacturing 7, 012010 (2024).

- ⁷Q. Shao, P. Li, L. Liu, H. Yang, S. Fukami, A. Razavi, H. Wu, K. Wang, F. Freimuth, Y. Mokrousov, M. D. Stiles, S. Emori, A. Hoffmann, J. Åkerman, K. Roy, J.-P. Wang, S.-H. Yang, K. Garello, and W. Zhang, IEEE Transactions on Magnetics **57**, 1 (2021).
- ⁸R. Saha, Y. P. Pundir, and P. Kumar Pal, Journal of Magnetism and Magnetic Materials 551, 169161 (2022).
- ⁹R. Ramaswamy, J. M. Lee, K. Cai, and H. Yang, Applied Physics Reviews 5, 031107 (2018).
- ¹⁰C. Song, R. Zhang, L. Liao, Y. Zhou, X. Zhou, R. Chen, Y. You, X. Chen, and F. Pan, Progress in Materials Science 118, 100761 (2021).
- ¹¹B. Dieny, I. L. Prejbeanu, K. Garello, P. Gambardella, P. Freitas, R. Lehndorff, W. Raberg, U. Ebels, S. O. Demokritov, J. Akerman, A. Deac, P. Pirro, C. Adelmann, A. Anane, A. V. Chumak, A. Hirohata, S. Mangin, S. O. Valenzuela, M. C. Onbasli, M. D'Aquino, G. Prenat, G. Finocchio, L. Lopez-Diaz, R. Chantrell, O. Chubykalo-Fesenko, and P. Bortolotti, Nature Electronics 3, 446 (2020).
- ¹²A. Slavin and V. Tiberkevich, IEEE Transactions on Magnetics 45, 1875 (2009).
- ¹³A. A. Tulapurkar, Y. Suzuki, A. Fukushima, H. Kubota, H. Maehara, K. Tsunekawa, D. D. Djayaprawira, N. Watanabe, and S. Yuasa, Nature 438, 339 (2005).
- ¹⁴S. Basak, S. Rajendran, S. Pollin, and B. Scheers, in 2021 International Conference on COMmunication Systems & NETworkS (COMSNETS) (IEEE, Bangalore, India, 2021) pp. 548–555.
- ¹⁵S. Nadj-Perge, S. M. Frolov, E. P. a. M. Bakkers, and L. P. Kouwenhoven, Nature 468, 1084 (2010).
- ¹⁶C. Kloeffel and D. Loss, Annual Review of Condensed Matter Physics 4, 51 (2013).
- ¹⁷L. Pan, Y. Xie, H. Yang, M. Li, X. Bao, J. Shang, and R.-W. Li, SENSORS 23, 4083 (2023).
- ¹⁸Y. Yang, Y. Xu, H. Xie, B. Xu, and Y. Wu, Applied Physics Letters 111, 032402 (2017).
- ¹⁹X. Chen, H. Xie, H. Shen, and Y. Wu, Physical Review Applied **18**, 024010 (2022).
- ²⁰H. Xie, X. Chen, Z. Luo, and Y. Wu, Physical Review Applied 15, 024041 (2021).
- ²¹R. Li, S. Zhang, S. Luo, Z. Guo, Y. Xu, J. Ouyang, M. Song, Q. Zou, L. Xi, X. Yang, J. Hong, and L. You, Nature Electronics 4, 179 (2021).
- Yang, J. Hong, and L. Tou, Nature Electronics 4, 179 (2021).
 M. Hassan, G. Abbas, N. Li, A. Afzal, Z. Haider, S. Ahmed, X. Xu, C. Pan, and Z. Peng, Advanced Materials Technologies 7, 2100773 (2022).
- ²³Z. Hui, L. Zhang, G. Ren, G. Sun, H.-D. Yu, and W. Huang, Advanced Materials 35, 2211202 (2023).
- ²⁴M. S. Kim, A. S. Almuslem, W. Babatain, R. R. Bahabry, U. K. Das, N. El-Atab, M. Ghoneim, A. M. Hussain, A. T. Kutbee, J. Nassar, N. Qaiser, J. P. Rojas, S. F. Shaikh, G. A. Torres Sevilla, and M. M. Hussain, Advanced Materials 36, 2406424 (2024).
- ²⁵R. Qin, J. Nong, K. Wang, Y. Liu, S. Zhou, M. Hu, H. Zhao, and G. Shan, Advanced Materials 36, 2312761 (2024).
- ²⁶M. Li, C. Li, X. Xu, M. Wang, Z. Zhu, K. Meng, B. He, G. Yu, Y. Hu, L.-M. Peng, and Y. Jiang, Nano Letters 23, 3818 (2023).
- ²⁷E. Liu, T. Fache, D. Cespedes-Berrocal, Z. Zhang, S. Petit-Watelot, S. Mangin, F. Xu, and J.-C. Rojas-Sánchez, Physical Review Applied 12, 044074 (2019).
- ²⁸G. D. Hwee Wong, Z. Xu, W. Gan, C. C. I. Ang, W. C. Law, J. Tang, W. Zhang, P. K. J. Wong, X. Yu, F. Xu, A. T. S. Wee, C. S. Seet, and W. S. Lew, ACS Nano 15, 8319 (2021).
- ²⁹Z. Zhang, E. Liu, W. Zhang, P. K. J. Wong, Z. Xu, F. Hu, X. Li, J. Tang, A. T. S. Wee, and F. Xu, ACS Applied Materials & Interfaces 11, 8258 (2019).
- ³⁰Z. Zhang, E. Liu, X. Lu, W. Zhang, Y. You, G. Xu, Z. Xu, P. K. J. Wong, Y. Wang, B. Liu, X. Yu, J. Wu, Y. Xu, A. T. S. Wee, and F. Xu, Advanced Functional Materials 31, 2007211 (2021).
- ³¹S. Hu, E. Liu, Y. Bai, M. Zhuang, W. Liu, M. Lei, Y. Zhang, G. Xu, F. Xu, and S. Mangin, Physical Review B 109, 224407 (2024).
- ³²H. Matsumoto, S. Ota, T. Koyama, and D. Chiba, Applied Physics Letters 118, 022406 (2021).
- ³³ H. Matsumoto, S. Ota, T. Koyama, and D. Chiba, Applied Physics Express 15, 033004 (2022).
- ³⁴D. Schwienbacher, M. Pernpeintner, L. Liensberger, E. R. J. Edwards, H. T. Nembach, J. M. Shaw, M. Weiler, R. Gross, and H. Huebl, Journal of

- Applied Physics 126, 103902 (2019).
- ³⁵ N. Nagaosa, J. Sinova, S. Onoda, A. H. MacDonald, and N. P. Ong, Reviews of Modern Physics 82, 1539 (2010).
- ³⁶W. Ju, M. Li, J. Chen, T. Li, X. Wang, D. Kang, H. Li, and B. Zhao, Applied Physics Letters 124, 142402 (2024).
- ³⁷H. Xie, J. Yuan, Z. Luo, Y. Yang, and Y. Wu, Scientific Reports 9, 17254 (2019).
- ³⁸B. Zhao, D. Khokhriakov, Y. Zhang, H. Fu, B. Karpiak, A. M. Hoque, X. Xu, Y. Jiang, B. Yan, and S. P. Dash, Physical Review Research 2, 013286 (2020).
- ³⁹C. Stamm, C. Murer, Y. Acremann, M. Baumgartner, R. Gort, S. Däster, A. Kleibert, K. Garello, J. Feng, M. Gabureac, Z. Chen, J. Stöhr, and P. Gambardella, Physical Review B 100, 024426 (2019).
- ⁴⁰Y.-G. Choi, D. Jo, K.-H. Ko, D. Go, K.-H. Kim, H. G. Park, C. Kim, B.-C. Min, G.-M. Choi, and H.-W. Lee, Nature 619, 52 (2023).
- ⁴¹W. Wang, T. Wang, V. P. Amin, Y. Wang, A. Radhakrishnan, A. Davidson, S. R. Allen, T. J. Silva, H. Ohldag, D. Balzar, B. L. Zink, P. M. Haney, J. Q. Xiao, D. G. Cahill, V. O. Lorenz, and X. Fan, Nature Nanotechnology 14, 819 (2019).